Princeton Plasma Physics Laboratory

PPPL- 4537

PPPL- 4537

Absolute Calibration of an Electrostatic Dust Detector

B. Rais, C.H. Skinner, A.L. Roquemore

July, 2010

Prepared for the U.S. Department of Energy under Contract DE-AC02-09CH11466.

Princeton Plasma Physics Laboratory
Report Disclaimers

Full Legal Disclaimer

Trademark Disclaimer

PPPL Report Availability

Princeton Plasma Physics Laboratory:

http://www.pppl.gov/techreports.cfm

Office of Scientific and Technical Information (OSTI):

http://www.osti.gov/bridge

Related Links:

U.S. Department of Energy

Office of Scientific and Technical Information

Fusion Links

Absolute Calibration of an Electrostatic Dust Detector

B. Rais[1], C.H. Skinner[2] A.L. Roquemore[2]

[1]*Université de Provence, Aix-Marseille, France*

[2]*Princeton Plasma Physics Laboratory, Princeton, N. J., 08543, USA*

Abstract

Methods to measure the inventory of dust particles and to remove dust if it approaches safety limits will be required in next-step tokamaks such as ITER. An electrostatic dust detector, based on a grid of interlocking circuit traces biased to 50 V, has been developed for the detection of dust on remote surfaces in air and vacuum environments. We report detailed measurements of the absolute calibration of the electrostatic dust detector. The sensitivity in vacuum for carbon particles with a count median diameter of 2.14 µm was found to be 0.15 ng/cm^2/count for a 51 mm detector with cover mesh in vacuum conditions, and for lithium particles of average diameter 44 µm is 14.5 ng/cm^2/count for a 13 mm detector without cover mesh in vacuum.

1. Introduction

High levels of dust are expected in next-step fusion devices because of the intense plasma-wall interactions and long pulse duration [1]. The dust can be radioactive from tritium or activated tungsten, toxic, and/or chemically reactive with steam or air and the accumulation of dust will have operational and potential safety impacts in four areas. To limit the radiological source term in case of accidental release to the environment the quantity of dust in ITER will be maintained below 1,000 kg [2]. An administrative limit of 670 kg is envisioned to take account of measurement uncertainties. Secondly, to limit the potential explosion hazard in case a coolant leak and simultaneous air ingress result in hydrogen generation from chemical reactions between dust on hot surfaces and steam/water, the quantity of dust on hot surfaces will be maintained below 6 kg of C and 6 kg of Be, or if C is absent, 11 kg of Be and 230 kg of W. Thirdly, dust transport to the core plasma will raise impurity concentrations, degrade fusion performance and may cause disruptions. Fourthly, dust may coat diagnostic mirrors necessary to monitor plasma operations and compromise their performance. The tolerable amount of dust for the last two issues is not known. Clearly dust detection and dust removal techniques will be vital to the operation of ITER and future fusion reactors.

The ITER strategy [2] includes indirect measurement of dust generation via measurements of the erosion of plasma facing components. Initially 100% of the erosion products will be conservatively assumed to be dust. Direct local measurements of dust are envisioned to provide information on dust generation on a pulse-by-pulse basis with a measurement requirement of 20% relative and 50% absolute accuracy. However dust measurement techniques are still in their infancy, especially for dust on hot surfaces. The first real-time measurement of surface dust in an operating tokamak using an electrostatic dust detector has been reported in ref. [3]. The device is designed to detect dust particles settling on a remote surface. Two closely interlocking combs of copper traces on a circuit board are biased at 50 V (Fig. 1). When a conductive dust particle settles on this surface a miniature spark is generated creating a transient short circuit and the resulting current pulse is detected electronically. At the same time the heat generated by the current vaporizes at least part of the particle causing it to rocket off the surface or vaporize. This restores the open circuit, resetting the detector for the next dust particle. The sensitivity of the

device was increased by four orders of magnitude to match the dust levels found in NSTX. At the same time, a differential detection electronics was implemented that made the detector largely immune to electrical noise in the tokamak environment [3].

We describe the absolute calibration of this detector for carbon and lithium particles. The physics of dust in plasmas has been reviewed in ref. [4] and previous work on dust diagnostic techniques has been recently reviewed in refs. [5,6].

2. Particle size characterization

The carbon particles used to test the detector were scraped from a spare NSTX ATJ graphite tile. To characterize the size distribution of the particles a sample was gently blown with a hand puffer onto a clean glass slide and viewed in a digital microscope with a 40x objective and pixel size of 0.17 µm [7]. Several digital images were combined into montages and the size distribution analyzed using ImageJ software [8]. This converted the gray-scale image into black and white and calculated the area of each particle. The black/white threshold was set visually so the smallest particles were visible, without adding artifacts. The projected area diameter, D, (diameter of a spherical particle with equivalent area) was derived from the area measured by ImageJ, using:

$$D = 2 \times \sqrt{Area/\pi}$$

The count median diameter was found to be 2.14 µm with a geometric standard deviation of 2.58 µm and diameter of average mass of 8.21 µm. This is similar to particles that had accumulated on a viewport at the bottom of the NSTX vessel that had a count median diameter of 2.06 µm [9] and to dust samples that were taken from several locations in the NSTX vessel with a vacuum pump and filter attachment that had an average count median diameter of 3.27 µm [10].

On NSTX a lithium aerosol is used to drop lithium particles into the plasma for wall conditioning purposes [11]. The particles are Stabilized Metallic Lithium Powder from FMC corporation (trade mark: SLMP). The manufacturer specifies a particle size of 44 µm average diameter with

a 40 nm coating of Li_2CO_3. A large signal from these particles was recorded by the electrostatic dust detector and hence the detector response to these particles was also measured.

3. Calibration procedure

The detector [12,13] is designed to detect dust particles settling on a remote surface. In the present embodiment two closely interlocking combs of copper traces on a circuit board are biased to 50 V (Fig. 1). When a conductive dust particle settles on this surface a miniature spark is generated creating a transient short circuit and the resulting current pulse is detected electronically. The short circuit is terminated approximately 1 µs later as the heat generated by the current vaporizes at least part of the particle causing it to rocket off the surface or vaporize. This restores the open circuit, and resets the detector for the next incident dust particle.

The particles were spread evenly over a dust tray that had a 22 mm square double or triple layer mesh bottom. The mesh pore size was 90 µm and the multiple layers helped retain the dust until needed. The tray was weighed with a Sartorius ME5-F microbalance with 1 µg resolution, 5 g capacity and 51 mm diameter pan that was recalibrated at least twice each day. The dust tray was weighed and then moved to a tray holder suspended below a 6" conflat flange with an aluminum foil disc underneath to catch any dust that fell through the mesh. The flange with the dust tray was then carefully placed on top of the test chamber above the dust detector (Fig. 2).

For experiments in vacuum, viton gaskets were used to seal the chamber and avoid the mechanical vibration associated with tightening copper gaskets. The chamber was evacuated to 50-100 mTorr. A baffle was installed over the evacuation port in the chamber to deflect air currents from the detector during evacuation or venting. To avoid disturbing the dust, pumping was done slowly over 3-5 min and then the pumping valve closed for dust measurements. Dust was delivered to the detector by mechanically knocking on the chamber or by using a vibrator and the response of the electronics recorded. After the measurement the chamber was vented if necessary and the dust tray transferred back to the balance for reweighing. Extreme care was used to get high accuracy measurements of the mass. Small temperature differences between the

weighed objects and the balance could cause air currents and stabilization times of 5-10 min. A reading was considered final when it was stable for more than 60 s.

The mass loss of the tray was determined by measuring the mass of tray, foil disk and dust before and after dust delivery. The accuracy of the mass measurements in both air and vacuum conditions was estimated by performing a weighing cycle without tapping the chamber to deliver dust. These showed a very small average mass loss of 0.93 µg ± 0.11 µg in air conditions and 2.6 µg ± 0.2 µg in vacuum that was subtracted from the calculated mass difference delivered to the detector. Extraneous dust was removed from the detector with compressed gas before every trial.

The detector was fabricated by photolithography on Ultralam substrates as in ref [14,15]. The traces and inter-trace space were 25 µm wide as before and the circuit could standoff at least 60 V. The response of the energized detector to dust was recorded using a differential detection electronics circuit that is shown schematically in Fig. 3. The detector is biased to 50 V through 25 resistors rated at 44 W, four times the maximum power that can be supplied in case of a complete short circuit. The balanced inputs from the detector are first attenuated by a factor 10 and input to an Analog Devices 10 MHz instrumentation amplifier, AD8250ARMEZ with a gain of unity. The amplifier is followed by a 200 ns low pass filter and a comparator that compares the signal to a reference trip point. This is currently set to 4.58 V and corresponds to a resistance between the detector traces of less than 480 Ω. The power supply current limit was set to 450 mA.

The dust was delivered to the detector by applying a vibrator tool to the flange at the top of the dust tower (Fig. 2) or by simply knocking on the flange with a wrench. The knocking method has potential for a large number of particles landing on the detector at the same instant with potential loss of signal due to pulse pileup issues. However a comparison of the two delivery methods (shown later in section 5 Fig. 7) showed that there was not a significant difference in the results from the two methods and hence pulse pileup is not an issue. The number of counts often continued incrementing slowly after the vibration ceased, especially for the larger quantities of dust. Dust detector data recorded with the NSTX data acquisition system is shown in Fig. 4 and

shows the signal extending over about 10 seconds from a single event (knock). In the calibration the final count was recorded when the count number stayed constant for at least 2 min.

Previously it was shown in ref. [16] that while up to 90% of the amount of dust incident on the energized detector was ejected or vaporized, about 10% could remain on the surface of the detector. In NSTX a stainless steel wire mesh with pore size 90 µm covered the detectors to prevent large debris and fibers from settling on the detector and potentially causing a permanent short circuit. Some calibrations were done with this mesh cover and a significant amount of dust was noticed remaining on the mesh wires. Vibrations alone (without any additional incident dust) could disturb residual dust on the detector or mesh and trigger additional counts even after the dust source was removed from the dust tower. That number was typically 10% but could be up to 150% when the mesh was used. The total number of counts plotted in the following figures includes the additional counts after the dust source was removed. The detector was cleaned with compressed gas in between each measurement. A helium puffing system [17] is under development to enable the removal of residual dust.

A series of calibration measurements were undertaken for different particles and different sized detectors in vacuum and air conditions.

4. Calibration results with a 51mm detector

The area on which the dust fell was measured by positioning white paper at the detector position. Most of the dust fell within a 25x25 mm square area so that a 51 mm square detector received all of the dust lost by the tray. The flux of particles landing on the detector is calculated from the mass loss of the dust tray divided by the area of the 51 mm detector. Fig. 5 shows the response of the 51 mm / 25 µm gap detector covered with the 90 µm pore mesh in vacuum conditions as used in NSTX. A least squares linear fit to the data was performed. The threshold sensitivity of the 51 mm detector to carbon particles was calculated from the fit to be 0.15 ng/cm^2/count in vacuum conditions with the mesh. The 51 mm detector was a factor-of-two more sensitive at atmospheric pressure with a threshold sensitivity of 0.078 ng/cm^2/count with the mesh. These

results are consistent with previous work [15,16] after applying factors to compensate for the different conditions (30 V bias, 50 mV threshold).

The 51 mm detector was also calibrated without the protection mesh in vacuum and in air at atmospheric pressure. The results are shown in Fig. 6 and the sensitivity without the mesh was found to be 0.049 ng/cm^2/count in air conditions and 0.10 ng/cm^2/count in vacuum. The use of the protection mesh changes the sensitivity by a factor similar to the 60% optical transmission of the mesh showing that some particles are left on the wires.

5. Results from calibration with a 13 mm detector

Calibration experiments were performed with 13 mm square detectors that are less expensive than the 51 mm detectors and are suitable for applications where the highest sensitivity is not required. These were fabricated by photolithography on Ultralam substrates with 25 µm wide traces and inter-trace space, just as the 51 mm detectors. The fraction of dust falling on the 13 mm square detector was measured with a 13 mm square tray at the detector position and was 28 % in both air and vacuum conditions. As a comparison, the geometric ratio between the surface area of the detector surface to area of the tray was 34 % indicating that some dust did not fall vertically.

Fig. 7 shows the response of the 13 mm square 25 µm spacing detector in vacuum conditions and without a mesh cover. A linear fit to the data shows a regression coefficient of $R^2 = 0.90$ and a sensitivity of 1.4 ng/cm^2/count. Two different dust delivery methods were used (vibro tool and knocking) but there is no systematic difference in the response. For comparison, Fig. 5a in ref. [15] also reports the response of this 13 mm detector, but at a lower bias voltage (30 V compared to 50 V) and lower SCA threshold (50 mV compared to 400 mV) and shows more scatter in the data. After applying factors to compensate for the different experimental conditions, and considering the higher scatter, the ref. [15] data is consistent with the more accurate data shown here.

Fig.8 shows the response of the 13 mm square 25 µm spacing detector in air at atmospheric pressure without a mesh cover. A linear fit to the data shows a regression coefficient of $R^2 = 0.98$

and a sensitivity of 0.63 ng/cm^2/count, indicating that the detector is a factor-of-two more sensitive in air than in vacuum. This is also consistent with the results of ref. [15] and confirms results from the calibration of the 51 mm detector. It can be seen that the 51 mm detector was 13x more sensitive than the 13 mm detector in both air and vacuum environments, a factor broadly consistent with the 16x increase in the area.

To check that the response per unit area of the 13 mm and 51 mm detectors was the same measurements were made with a 13 mm square mask over the 51 mm detector at atmospheric pressure. The results (Fig. 9) confirm that the response per unit area of the different sized detectors is the same as expected.

6. Calibration of the 13 mm detector with lithium particles

Lithium particles are used for wall conditioning in NSTX [11] and one of the two sources of the Li particles is in a port directly above the dust detector. A dramatic increase in dust detector signal in NSTX was observed coincident with the operation of the Li particle source [3]. This detector response to lithium particles is also interesting as lithium can also be considered as a proxy for beryllium particles that may be generated in ITER.

The dust detector calibration was performed with the 44 µm diameter lithium particles that were also used for NSTX wall conditioning [10]. Fig. 10 shows the response of a 13 mm / 25 µm gap detector in vacuum to the incident lithium particles. The sensitivity in vacuum without mesh cover was measured to be 14.5 ng/cm^2/count. The lower sensitivity of the lithium particles compared to carbon particles is consistent with the smaller detector used and the decrease in sensitivity with increasing size of particles reported in ref. [13].

Special precautions were needed to handle the lithium powder as lithium reacts violently with water to give off corrosive dust and flammable hydrogen gas and an elevated temperature can result in spontaneous ignition in humid air. To mitigate these hazards a mask, gloves, protection glasses and an anti-fire coat were used to prevent inhaling or having eye contact with lithium powder. Also lithium oxidizes upon exposure to air changing the mass. To minimize mass changes due to oxidation the equipment was moved to an argon filled glove box. The argon

atmosphere minimized the oxidation of the lithium particles during handling. Argon was flowed into the glove box for about two hours before the experiment and the humidity inside the box decreased from 55% to 10% indicating most of the air had been displaced. The detector was cleared of residual dust with an argon puff instead of using the compressed gas.

The change in mass due to exposure to residual oxygen during the transfer from the balance to the vacuum chamber and back was tracked for each measurement. This correction is of order 9% and was subtracted from the final mass. Care had to be taken with the evacuation and the venting of the chamber as lithium powder is very light and gas currents in the chamber could transfer the powder to the detector. Li particles were delivered to the detector by 20-40 knocks with a small hammer on the top flange of the chamber. Lithium particles flowed more easily through the mesh than carbon particles and extreme care was needed when the flange was bolted on or removed, as even a very weak vibration could trigger the release of particles. After the calibration the chamber was vented with argon.

After 4 trials the detector response became unstable even a long time [≈5 min.] after the dust source was removed because of the increasing amount of residual lithium particles remaining. 6107 counts were observed after the dust tray was removed in the 5^{th} trial and this amount was subtracted from the 265 $\mu g/cm^2$ point in Fig. 10.

Lithium is known to react chemically with copper, and an inspection of the detector traces after the experiment showed that the detector traces were covered by a small layer of passivated lithium. In future work a helium gas puffing system such as described in ref. [17] will be added to periodically clear residual particles remaining on the detector.

7. Comparison of unipolar and differential electronics

The initial use of the dust detector in NSTX showed strong electromagnetic interference from the RF antennas and switched power amplifiers (SPA) that complicated the identification of signals from dust. To avoid this interference the detection electronics was changed from the unipolar system used in ref. [15] to a new differential detection electronics circuit described in sect. 3 and shown schematically in Fig. 3. A comparison of the response of the 13 mm detector without

cover mesh in vacuum using the differential electronics to data previously taken with the unipolar electronics [15] was made. In Fig. 5a of ref. [15] the response was recorded in air at atmospheric pressure with the unipolar electronics at a lower bias voltage (30 V compared to 50 V) and lower SCA threshold (50 mV compared to 400 mV). After applying factors to compensate for the different experimental conditions, the data was plot in Fig. 11 together with the present results in the same conditions with the differential electronics from Fig. 7. A linear fit to the data indicates a 50% larger slope for the differential electronics, but this difference is within the scatter of the previous measurement.

8. Reducing the gap between detector traces

For environments with a high dust flux a lower sensitivity detector may be required. This can be achieved with a coarser detector spacing as reported previously in ref. [12]. To measure the sensitivity of a coarse detector spacing with the new differential electronics, the calibration was conducted with a 13 mm detector with 127 µm wide traces and a 127 µm gap between the traces. Fig. 12 compares the response in vacuum conditions of the 13 mm / 127 µm gap detector and the 13 mm / 25 µm gap data from Fig. 7. The sensitivity of the 13 mm / 127 µm gap detector was 7.8 ng/cm^2/count compared to 1.4 ng/cm^2/count with the 25 µm gap.

The results showed that as the spacing of the detector increases, the detector becomes less sensitive to dust. Detectors with larger gap and more rugged and thicker traces can also provide readings of much larger amounts of particles without risking a continuous short circuit [13]. This would be advantageous for ITER where lower sensitivity would appropriate as the dust levels are much higher than the levels in existing tokamaks.

9 Conclusion

The electrostatic dust detector has been calibrated with carbon and lithium particles under various conditions and the results are summarized in Table 1. The detector is now sufficiently sensitive for measurements on contemporary tokamaks as was demonstrated in ref. [3]. Some results from a more rugged detector with coarse spacing were presented above. We note that development work remains to make these detectors compatible with the harsh ITER in-vessel

environment and suitable for tungsten particles. In addition the detector will need to be fabricated from radiation resistant materials and operate reliably for long periods without maintenance.

Table 1

Material	Detector size	Air/vacuum	Cover mesh	Sensitivity $ng/cm^2/count$
Carbon	51 mm	Vacuum	No	0.10
Carbon	51 mm	Air	No	0.049
Carbon	51 mm	Vacuum	Yes	0.15
Carbon	51 mm	Air	Yes	0.078
Carbon	13 mm	Vacuum	No	1.4
Carbon	13 mm	Air	No	0.63
Lithium	13 mm	Vacuum	No	14.5

Acknowledgements

The authors would like to thank National Undergraduate Fellows: A. Bader, D. Boyle, A. Campos, C. Parker, R. Hensley, C. Voinier for previous work and C. Bunting, M. Cropper, and T. Holoman for technical assistance. We are indebted to D. Mansfield for assistance in handling the lithium particles. This work was funded by US DOE Grant No DE AC02-09CH11466.

Figure Captions

Fig. 1: Schematic of dust detector (not to scale) showing interlocking combs of traces. Dust impinging on the traces causes a short circuit and a voltage signal is generated across the 51 ohm resistor.

Fig. 2: Dust tray stand and dust tower used to deposit microgram quantities of dust on electrostatic detector.

Fig. 3: Schematic of the differential detection circuit

Fig. 4: Signal generated by laboratory dust source incident on detector as recorded by the NSTX data acquisition system.

Fig. 5: Response of the 51x51 mm / 25 µm spacing detector in vacuum conditions. The line is a linear fit to the data of slope 0.15 ng/cm^2/count and the R^2 = 0.98 is the regression coefficient.

Fig. 6: Response of the 51x51 mm / 25 µm spacing detector in vacuum conditions (triangles) and in air at atmospheric pressure (squares). The lines are linear fits to the data corresponding to sensitivity of 0.049 ng/cm^2/count (air) and 0.10 ng/cm^2/count (vacuum). R^2 is the regression coefficient.

Fig. 7: Response of the 13x13 mm / 25 µm spacing detector in vacuum conditions. The line is a linear fit of slope 1.4 ng/cm^2/count and R^2 = 0.90 is the regression coefficient of the data. The data labels distinguish two different dust delivery methods (vibro tool or knocks) and there is no noticeable difference in the response.

Fig. 8: Response of the 13x13 mm / 25 µm spacing detector in air conditions. The line is a linear fit to the data of slope 0.63 ng/cm^2/count and the R2 = 0.98 is the regression coefficient of the data.

Fig. 9: Response of the 51mm detector with a 13 mm aperture compared to the response of the 13 mm detector in air conditions (data from Fig. 7). The lines are linear fits to the data with the equation shown and the R^2 is the regression coefficient of the data.

Fig. 10: Response of the 13x13 mm / 25 µm spacing detector in vacuum to 44 µm Li particles. The line is a linear fit to the data of slope 14.5 ng/cm^2/count and the R^2 = 0.98 is the regression coefficient.

Fig. 11: Comparison of response of the 13 mm detector in vacuum using the differential electronics with previous data from ref. [15] taken with unipolar electronics (see text). The lines are linear fits and the R^2 is the regression coefficient of the data.

Fig. 12: Response of 13x13 mm detector 127 µm spacing (diamond) and 25 µm spacing (square points). The lines are linear fits and the R^2 is the regression coefficient of the data.

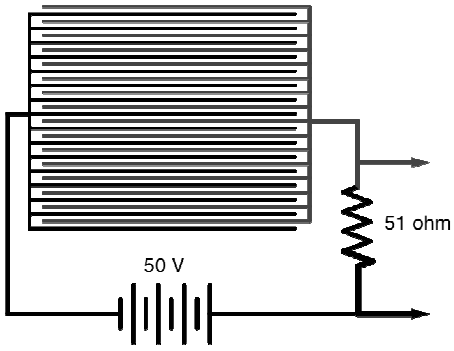

Fig. 1: Schematic of the dust detector (not to scale) showing interlocking combs of traces. Dust impinging on the traces causes a short circuit and a voltage signal is generated across the 51 ohm resistor.

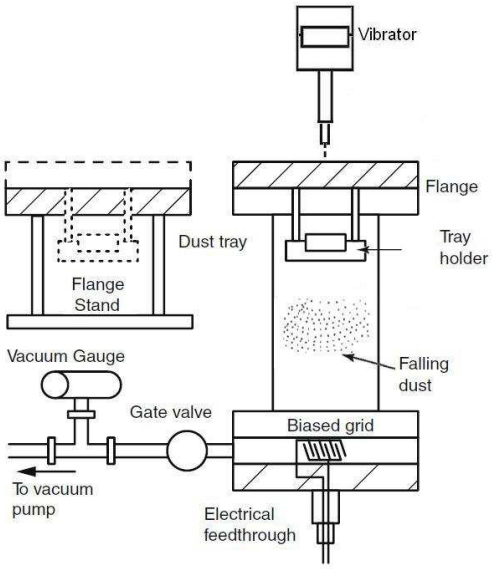

Fig. 2: Dust tray stand and dust tower used to deposit microgram quantities of dust on electrostatic detector.

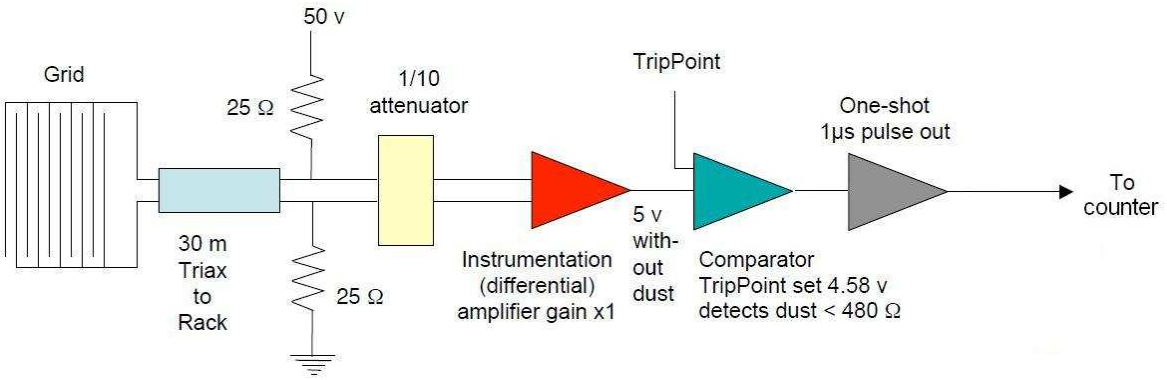

Fig. 3: Schematic of the differential detection circuit

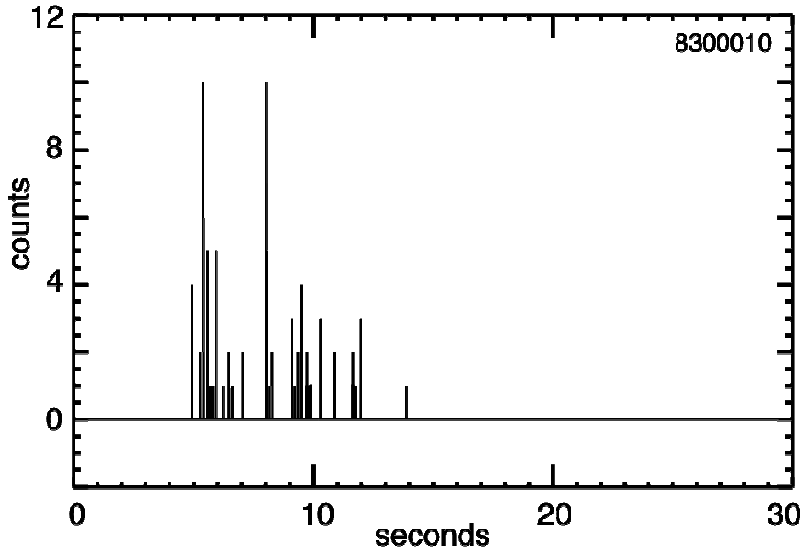

Fig. 4: Signal generated by laboratory dust source incident on detector as recorded by the NSTX data acquisition system.

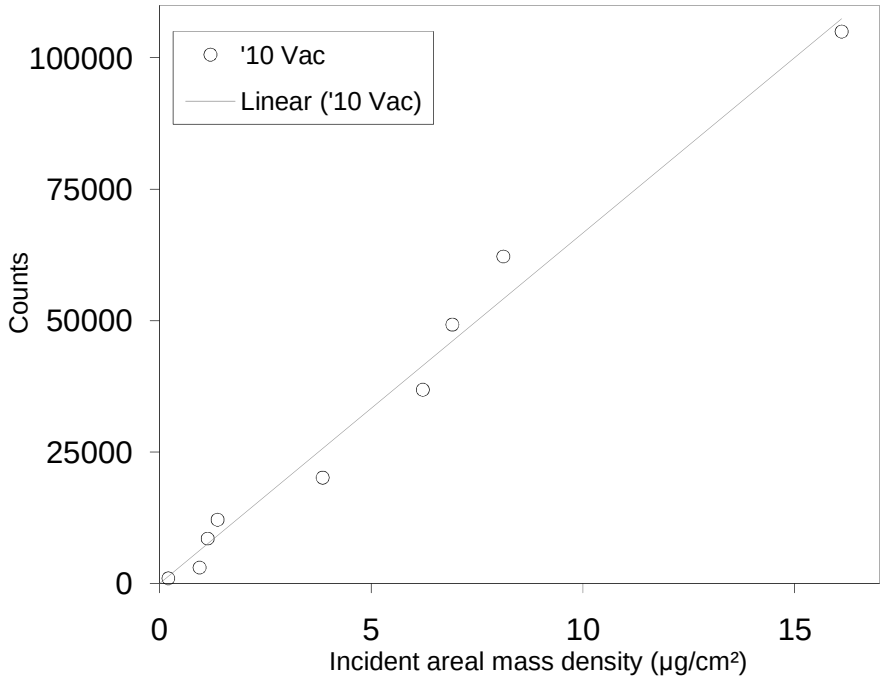

Fig. 5: Response of the 51x51 mm / 25 µm spacing detector in vacuum conditions. The line is a linear fit to the data of slope 0.15 ng/cm^2/count and the $R^2 = 0.98$ is the regression coefficient.

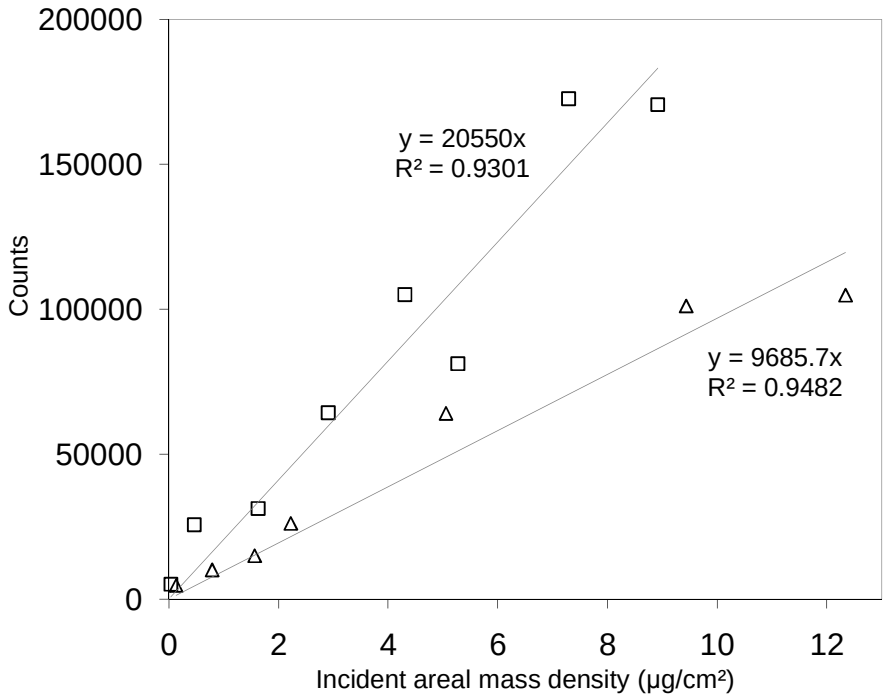

Fig.6: Response of the 51x51 mm / 25 µm spacing detector in vacuum conditions (triangles) and in air at atmospheric pressure (squares). The lines are linear fits to the data corresponding to sensitivity of 0.049 ng/cm^2/count (air) and 0.10 ng/cm^2/count (vacuum). R^2 is the regression coefficient.

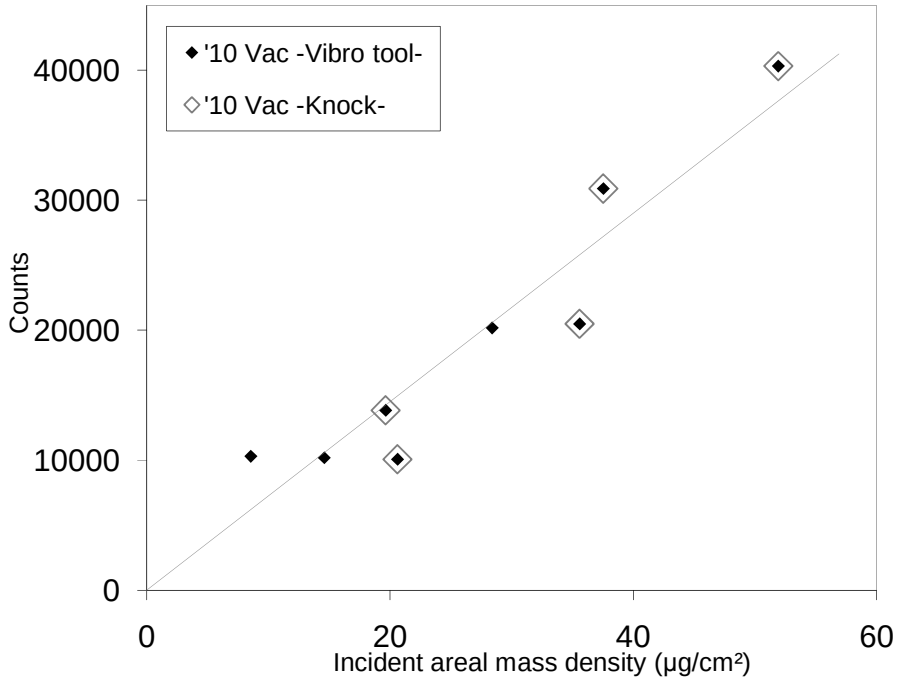

Fig. 7: Response of the 13x13 mm / 25 µm spacing detector in vacuum conditions. The line is a linear fit of slope 1.4 ng/cm^2/count and R^2 = 0.90 is the regression coefficient of the data. The data labels distinguish two different dust delivery methods (vibro tool or knocks) and there is no noticeable difference in the response.

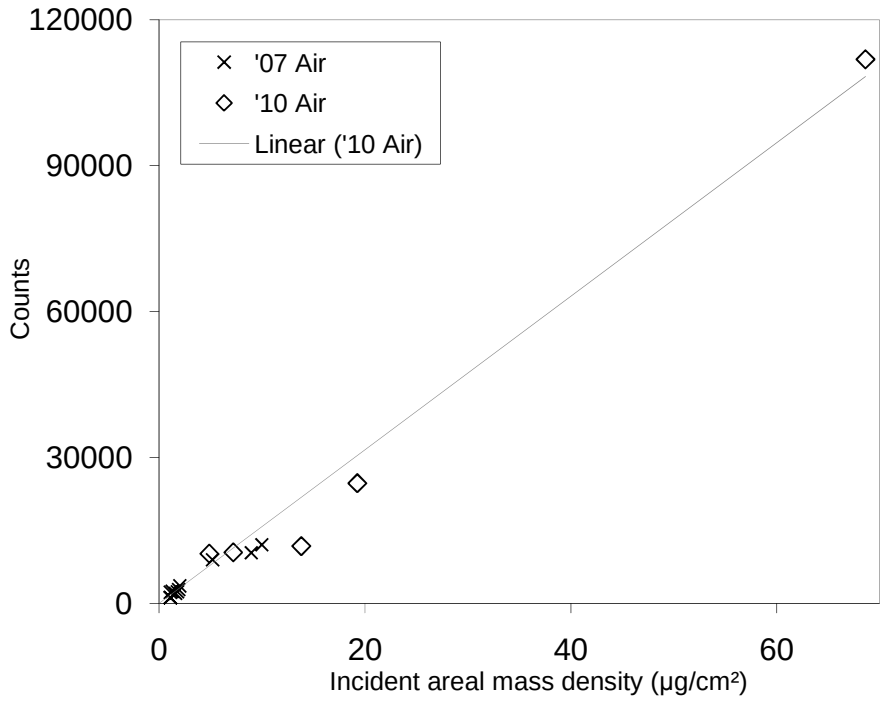

Fig.8: Response of the 13x13 mm / 25 µm spacing detector in air conditions. The line is a linear fit to the data of slope 0.63 ng/cm^2/count and the R^2 = 0.98 is the regression coefficient of the data.

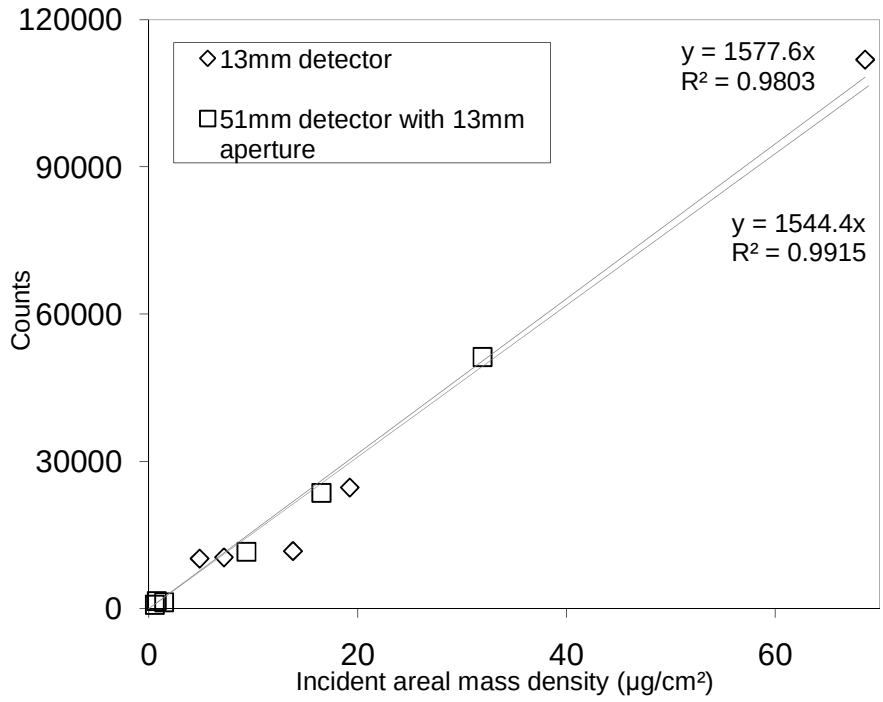

Fig. 9: Response of the 51mm detector with a 13 mm aperture compared to the response of the 13 mm detector in air conditions (data from Fig. 7). The lines are linear fits to the data with the equation shown and the R^2 is the regression coefficient of the data.

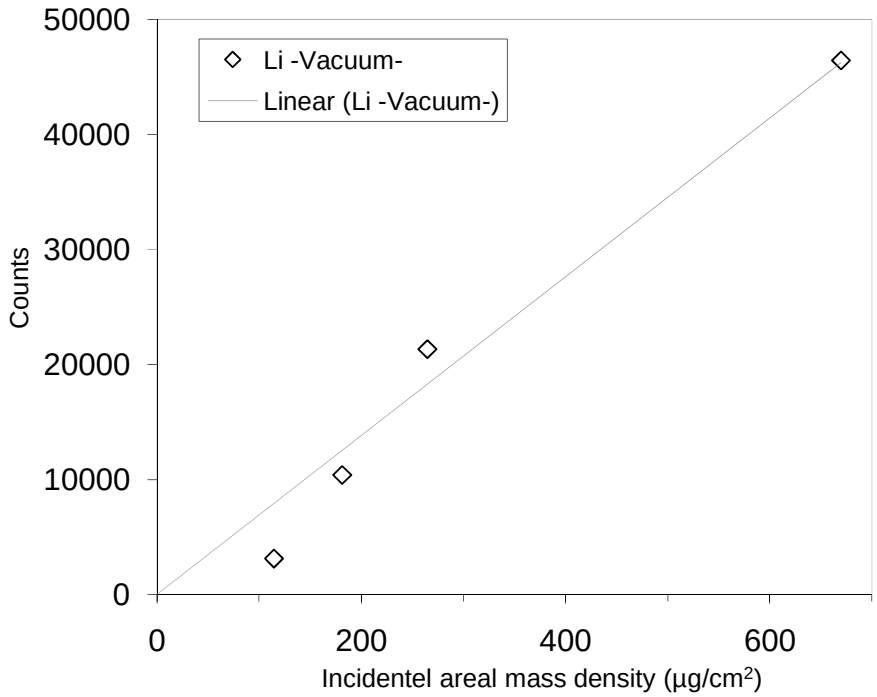

Fig. 10: Response of the 13x13 mm / 25 µm spacing detector in vacuum to 44 µm Li particles. The line is a linear fit to the data of slope 14.5 ng/cm^2/count and the R^2 = 0.97 is the regression coefficient.

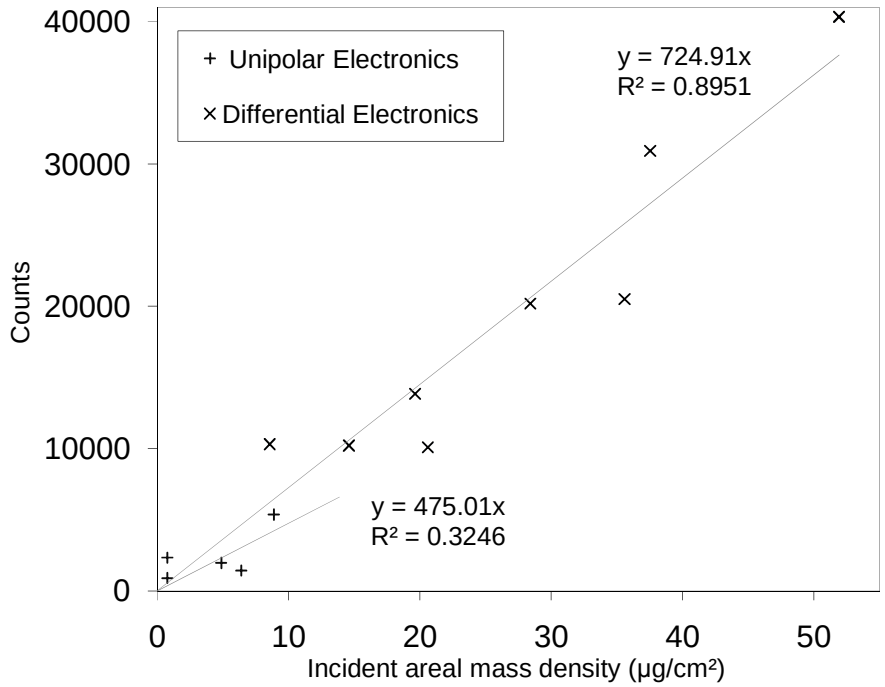

Fig. 11: Comparison of response of the 13 mm detector in vacuum using the differential electronics with previous data from ref. [15] using unipolar electronics (see text). The lines are linear fits and the R^2 is the regression coefficient of the data.

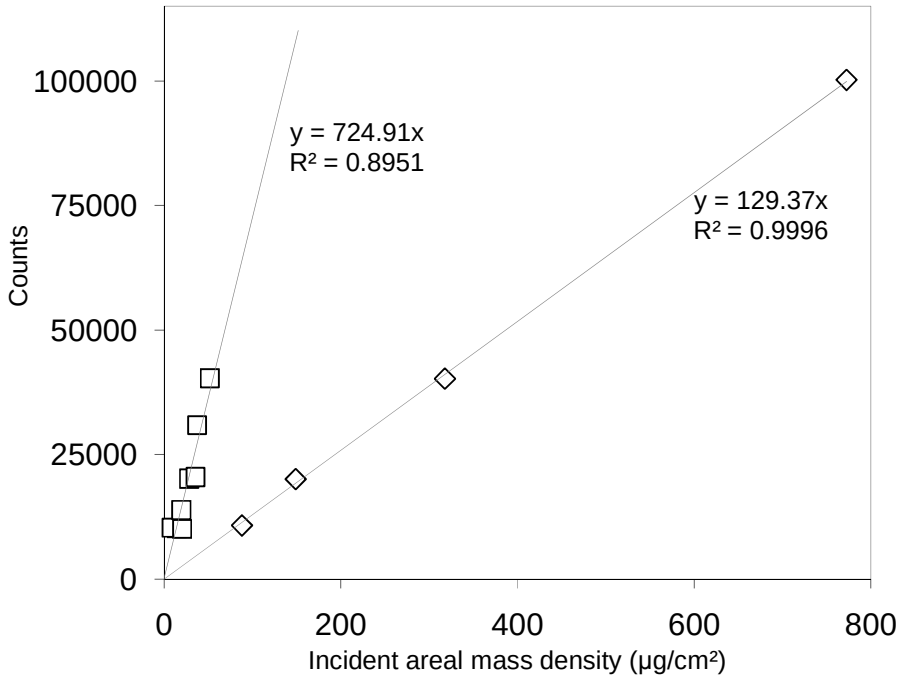

Fig. 12: Response of 13x13 mm detector 127 µm spacing (diamond) and 25 µm spacing (square points). The lines are linear fits and the R^2 is the regression coefficient of the data.

References

[1] G. Federici, C.H. Skinner, J.N. Brooks, J.P. Coad, C. Grisolia, A.A. Haasz, A. Hassanein, V. Philipps, C.S.Pitcher, J. Roth, W.R. Wampler, and D.G. Whyte, Nucl. Fus., 41, 1967 (2001).

[2] S. Rosanvallon, C. Grisolia, P. Andrew, S. Ciattaglia, P. Delaporte, D. Douai, D. Garnier, E. Gauthier, W. Gulden S.H. Hong, S. Pitcher, L. Rodriguez, N. Taylor, A. Tesini, S. Vartanian, A. Vatry, and M. Wykes, J. Nucl. Mater., 390-391 (2009) 57.

[3] C.H. Skinner, B. Rais, A. L. Roquemore, H.W. Kugel, R. Marsala, T. Provost ”First real-time detection of surface dust in a tokamak” PPPL report 4517 May 2010, Rev. Sci. Instrum. (2010) in press.

[4] S.I. Krasheninnikov A.Yu Pigarov, R.D. Smirnov, M. Rosenberg, Y. Tanaka, D.J. Benson, T.K. Soboleva, T.D. Rognlien, D.A. Mendis, B.D. Bray, D.L. Rudakov, J.H. Yu, W.P. West, A.L. Roquemore, C.H. Skinner, J.L. Terry, B. Lipschultz, A. Bader, R.S. Granetz, C.S. Pitcher, N. Ohno, S. Takamura, S. Masuzaki, N. Ashikawa, M. Shiratani, M. Tokitani, R. Kumazawa, N. Asakura, T. Nakano, A.M. Litnovsky, R. Maqueda and the LHD Experimental Group , Plasma Phys. Control. Fus. 50 (2008) 124054.

[5] C.J. Lasnier, S.L. Allen, J.A. Boedo, M. Groth, N.H. Brooks, A. McLean, B. LaBombard, C.H. Skinner, D.L. Rudakov, W.P. West, and C.P.C. Wong, , Fus. Sci. and Technol. 53 (2008) 640.

[6] D.L. Rudakov J.H. Yu, J.A. Boedo, E.M. Hollmann, S.I. Krasheninnikov, R.A. Moyer, S.H. Muller, A.Yu. Pigarov, M.Rosenberg, R.D. Smirnov,W.P.West, R.L. Boivin, B.D. Bray, N.H. Brooks, A.W. Hyatt, C.P.C.Wong, A.L. Roquemore, C.H. Skinner, W.M. Solomon, S. Ratynskaia, M.E. Fenstermacher, M. Groth, C.J. Lasnier, A.G. McLean, and P. C. Stangeby, Rev. Sci. Instrum., 79

[7] National Instruments model DC5-163 http://nationaloptical.com/.

[8] Available from: http://rsbweb.nih.gov/ij/.

[9] C.H. Skinner A.L. Roquemore, A. Bader, W.R. Wampler, Rev. Sci. Instrum., 75 (2004) 4213.

[10] J.P. Sharpe P.W. Humrickhouse, C.H. Skinner, T. Tanabe, K. Masaki, N. Miya, A. Sagara, J. Nucl. Mater., 337-339 (2000) 1000.

[11] D.K. Mansfield A.L Roquemore, H. Schneider, J. Timberlake, H. Kugel, M.G. Bell and the NSTX research team., Proceedings of the 2nd NIFS-CRC International Symposium on Plasma-Surface Interactions NIFS, Toki, Gifu, Japan January 18-20, 2010, to be published in Fus. Eng. & Des. [14] C. Voinier C.H. Skinner, A.L. Roquemore, J. Nucl. Mater., 346 (2005) 266.

[12] A. Bader C.H. Skinner, A.L. Roquemore, and S. Langish, Rev. Sci. Instrum., 75 (2004) 370.

[13] C. Voinier, C.H. Skinner, A.L. Roquemore, J. Nucl. Mater., 346 (2005) 266.

[14] C.H. Skinner, R. Hensley and A.L. Roquemore, J. Nucl. Mater., 376 (2008) 29.

[15] D.P. Boyle, C.H. Skinner, A.L. Roquemore, J. Nucl. Mater., 390-391 (2009) 1086

[16] C.V. Parker, C.H. Skinner and A.L. Roquemore, J. Nucl. Mater., 363- 365 (2007) 1461.

[17] A. Campos and C.H. Skinner, J. of Undergraduate Research IX (2009) 30. Available at http://www.scied.science.doe.gov/scied/JUR_v9/default.htm.

The Princeton Plasma Physics Laboratory is operated
by Princeton University under contract
with the U.S. Department of Energy.

Information Services
Princeton Plasma Physics Laboratory
P.O. Box 451
Princeton, NJ 08543

Phone: 609-243-2245
Fax: 609-243-2751
e-mail: pppl_info@pppl.gov
Internet Address: http://www.pppl.gov